

Gaped graphene bilayer: disorder and magnetic field effects

Eduardo V. Castro¹, N. M. R. Peres², J. M. B. Lopes dos Santos¹

¹CFP and Departamento de Física, Faculdade de Ciências Universidade do Porto, P-4169-007 Porto, Portugal and
²Center of Physics and Departamento de Física, Universidade do Minho, P-4710-057, Braga, Portugal

Double layer graphene is a gapless semiconductor which develops a finite gap when the layers are placed at different electrostatic potentials. We study, within the tight-binding approximation, the electronic properties of the gaped graphene bilayer in the presence of disorder, perpendicular magnetic field, and transverse electric field. We show that the gap is rather stable in the presence of diagonal disorder. We compute the cyclotron effective mass in the semi-classical approximation, valid at low magnetic fields. Landau level formation is clearly seen in zigzag and armchair ribbons of the gaped bilayer at intermediate magnetic fields.

I. INTRODUCTION

Graphene, the two-dimensional allotropic form of carbon, has recently deserved considerable attention. The realization that graphene could be obtained and studied experimentally revealed a plethora of unusual properties that may be useful in the design of new electronic devices [1–3]. The peculiar band structure of graphene, where at the corners of the Brillouin zone (BZ) the excitations are massless Dirac fermions, is responsible for many of the unconventional properties [4].

The possibility of creating stacks of graphene layers with the accuracy of a single atomic layer, providing an extra dimension to be explored, is another advantage of graphene for electronic applications. In particular, bilayer graphene has shown to have unusual electronic properties, though unexpectedly dissimilar to those exhibited by its single layer parent. The new type of integer quantum Hall effect observed in bilayer graphene [5, 6], which is induced by chiral parabolic bands, is an example of its uniqueness. Recent advances on the experimental side made it possible to produce bilayers where the two layers are effectively at different electrostatic potentials [7, 8] – introducing the concept of *biased bilayer*. This asymmetry between layers opens a gap between valence and conduction bands, which, in the unbiased case (both layers at the same potential), touch in a parabolic way at zero energy. The gap is a function of the potential between layers, and may be controlled by changing the electric field across the bilayer. This switching functionality opens the door for potential applications of bilayer graphene on atomic-scale electronic devices [9].

In this paper we study the biased bilayer system starting from the simplest tight-binding model. By computing the density of states (DOS) we analyze how the gap structure evolves when diagonal disorder is present. In the presence of a perpendicular magnetic field we obtain the cyclotron effective mass (semi-classical approximation), and study the Landau level formation in zigzag and armchair ribbons of bilayer graphene. The paper is organized as follows: in Sec. II we present the tight-binding Hamiltonian we use and discuss basic aspects of the electronic structure; the effect of disorder in the gap structure is discussed in Sec. III; in Sec. IV we analyze the effects of a perpendicular magnetic field; and Sec. V contains our conclusions.

II. MODEL AND BASIC ELECTRONIC STRUCTURE

In single layer graphene the carbon atoms form a honeycomb lattice which has two atoms per unit cell. These two atoms belong to different triangular lattices labeled A and B. The bilayer is made of two layers, which we label 1 and 2, arranged in the Bernal stacking (A1-B2). The unit cell has then four atoms, one per layer per sublattice. Each carbon atom contributes with a π electron, and thus the system is naturally at half-filling.

In the tight-binding approximation the relevant energy scales are the in-plane hopping energy, $t \approx 2.7$ eV, and the interlayer hopping energy, $t_{\perp} \approx 0.35$ eV. When a perpendicular magnetic field $\mathbf{B} = B \hat{e}_z$ is applied to the system t_{\perp} is unaffected but t acquires a phase [10] such that, $t \rightarrow t e^{i \frac{e}{\hbar} \int_{\mathbf{R}}^{\mathbf{R}+\delta} \mathbf{A} \cdot d\mathbf{r}}$, where e is the electron charge, δ is a vector connecting nearest-neighbor sites, and \mathbf{A} is the vector potential. The tight-binding Hamiltonian describing non-interacting π electrons in bilayer graphene then reads:

$$\begin{aligned}
 H = & -t \sum_{m,n} \left[e^{i\pi \frac{\phi}{\phi_0} n} a_{1,(m,n)}^{\dagger} b_{1,(m,n)} + e^{-i\pi \frac{\phi}{\phi_0} n} a_{1,(m,n)}^{\dagger} b_{1,(m-1,n)} + a_{1,(m,n)}^{\dagger} b_{1,(m,n-1)} + \text{h.c.} \right] \\
 & -t \sum_{m,n} \left[e^{-i\pi \frac{\phi}{\phi_0} (n-\frac{1}{3})} b_{2,(m,n)}^{\dagger} a_{2,(m,n)} + e^{i\pi \frac{\phi}{\phi_0} (n-\frac{1}{3})} b_{2,(m,n)}^{\dagger} a_{2,(m+1,n)} + b_{2,(m,n)}^{\dagger} a_{2,(m,n+1)} + \text{h.c.} \right] \\
 & -t_{\perp} \sum_{m,n} \left[a_{1,(m,n)}^{\dagger} b_{2,(m,n)} + \text{h.c.} \right] + \frac{V}{2} \sum_{m,n} \left[n_{A1,(m,n)} + n_{B1,(m,n)} - n_{A2,(m,n)} - n_{B2,(m,n)} \right],
 \end{aligned} \tag{1}$$

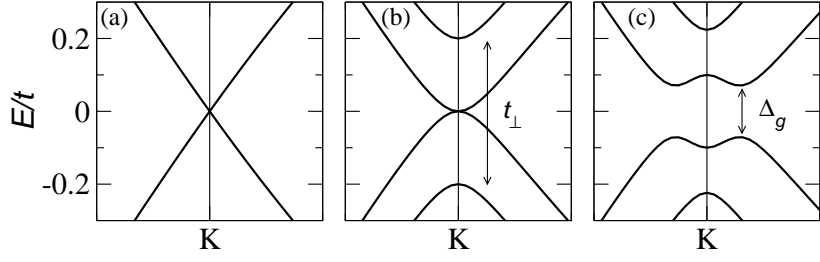


FIG. 1: Band structure of single layer graphene (a), unbiased bilayer graphene (b), and biased bilayer (c) with $V = 2t_{\perp}$, along two directions in the BZ near the Dirac (K) points. The inter-layer hopping was set to $t_{\perp}/t = 0.2$.

where $a_{i,(m,n)}^{\dagger}$ [$a_{i,(m,n)}$] and $b_{i,(m,n)}^{\dagger}$ [$b_{i,(m,n)}$] creates (annihilates) an electron on atom Ai and Bi of layer i at cell (m, n) , respectively. Spin indices have been neglected for simplicity. The Peierls phase in Eq. (1) is written assuming a Landau gauge, $\mathbf{A} = (-y, 0, 0)B$, where $\phi/\phi_0 = BA_{\square}/\phi_0$ is the magnetic flux through a plaquette in units of the flux quantum $\phi_0 = h/e$ (A_{\square} being the area of the graphene unit cell). The last term in Eq. (1) stands for the electrostatic potential difference, V , between the two layers, with $n_{Ai,(m,n)}$ and $n_{Bi,(m,n)}$ number operators.

The first (or second) line of Eq. (1) describes π electrons on single layer graphene. The resultant dispersion relation is given by,

$$\epsilon_{\mathbf{k}}^2/t^2 = 3 + 2 \cos(ak_x) + 4 \cos(ak_x/2) \cos(ak_y\sqrt{3}/2), \quad (2)$$

where a is the in-plane C-C distance for sites of the same sublattice. The vertex of the valence and conduction bands touch at the corners of the BZ (Dirac points), as shown in Fig. 1 (a). A Dirac linear dispersion follows at low energies, $\epsilon(q) = \pm v_F \hbar q$, where $v_F = t a \hbar^{-1} \sqrt{3}/2$ is the Fermi velocity which substitutes the speed of light, and \mathbf{q} is the wave vector relatively to the Dirac points. Taking into account the full Hamiltonian given in Eq. (1) we obtain four bands with dispersion energies given by,

$$E_{\mathbf{k}}^{\pm\pm}(V) = \pm \sqrt{\epsilon_{\mathbf{k}}^2 + t_{\perp}^2/2 + V^2/4} \pm \sqrt{t_{\perp}^4/4 + (t_{\perp}^2 + V^2)\epsilon_{\mathbf{k}}^2}, \quad (3)$$

with $\epsilon_{\mathbf{k}}$ as in Eq. (2). For the unbiased case Eq. (3) reduces to $E_{\mathbf{k}}^{\pm\pm} = \pm(\epsilon_{\mathbf{k}}^2 + t_{\perp}^2/4)^{1/2} \pm t_{\perp}/2$, from which it becomes clear that the spectrum is as in Fig. 1 (b): two low energy gapless bands touching in a parabolic way at the Dirac points, and two high energy bands with a gap of t_{\perp} . As the undoped bilayer is at half-filling, the Fermi energy (E_F) occurs at exactly at the points the bands $E_{\mathbf{k}}^{\pm-}$ touch. Thus, low energy quasi-particles are massive Dirac fermions with effective mass given by $m^* = 2t_{\perp}\hbar^2/3a^2t^2$ [6, 11]. The biased bilayer, however, shows a true gap between valence and conduction bands, as shown in Fig. 1 (c), and the low energy bands have a ‘‘Mexican hat’’ like dispersion. For $V \ll t$, which is the case for the biased bilayer, the gap behaves as $\Delta_g = [t_{\perp}^2 V^2 / (t_{\perp}^2 + V^2)]^{1/2}$, and is therefore fully controlled by the bias V .

III. EFFECT OF DIAGONAL DISORDER IN THE GAPPED STRUCTURE

Recent experiments using angle-resolved photoemission spectroscopy (ARPES) have clearly shown that the spectrum of the biased bilayer is well described by Eq. (3) [8], with the measured energy-momentum dispersion in good agreement with Fig. 1 (c). However, the experimental data also shows the presence of a finite spectral weight inside the gap, which may be attributed to disorder. The sources of disorder in the biased bilayer are not yet understood. Inhomogeneities in the substrate, below the bottom layer, as well as in the dopant coverages, above the top layer, are plausible sources. Here we consider the biased bilayer in the presence of diagonal disorder, adding the term $H_{\text{dis}} = \sum_{m,n,i=1,2} \varepsilon_{i,(m,n)} [n_{Ai,(m,n)} + n_{Bi,(m,n)}]$ to Eq. (1). We use the box distribution function to generate the random on-site energies, $\varepsilon \in [-W/2, W/2]$, and vary its width W in order to induce spectral weight inside the unperturbed gap.

To study how diagonal disorder affects the gap, and in particular how W compares with the other energy scales of the system, we have computed the DOS with the recursion method [12]. We define zero temperature retarded Green’s functions in the standard way,

$$G_{\mathbf{r}\mathbf{r}'}^{aa,i}(t) = -i \langle 0 | \{ a_{i,\mathbf{r}}(t), a_{i,\mathbf{r}'}^{\dagger}(0) \} | 0 \rangle \Theta(t), \quad G_{\mathbf{r}\mathbf{r}'}^{bb,i}(t) = -i \langle 0 | \{ b_{i,\mathbf{r}}(t), b_{i,\mathbf{r}'}^{\dagger}(0) \} | 0 \rangle \Theta(t), \quad (4)$$

where $\mathbf{r} = (m, n)$ specifies the cell. The recursion method gives an approximate value for the retarded Green’s function in the thermodynamic limit, and therefore for the disordered DOS, by simulating large lattices. The disorder averaged DOS is then easily obtained by averaging over disorder realizations.

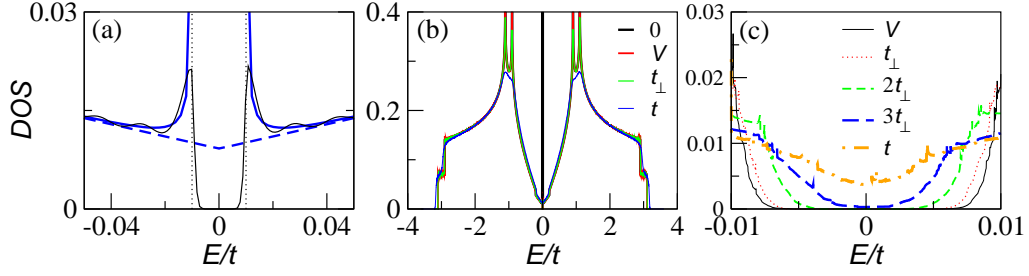


FIG. 2: (Color online) (a) - Non-disordered DOS: exact (thick lines) and recursion method result (normal line). (b) - DOS for several values of disorder W . (c) - The same as in (b) closer to the gap region.

Figure 2 resumes the results we have obtained for the effect of diagonal disorder in the DOS, with emphasis in the gap behavior. The simulated lattices had $2d^2$ sites, with $d = 1280$, and we averaged over 100 disorder realizations. The inter-layer hopping was set to $t_{\perp}/t = 0.2$. The bias was fixed to $V/t = 0.02$, as experimentally it is the smallest energy scale, $V \ll t_{\perp}$, and thus the gap is essentially the bias, $\Delta_g \approx V$. In order to check the performance of the recursion method in describing such a tiny region of the spectrum ($\Delta_g \ll t_{\perp} \ll t$), we show in Fig. 2 (a) the exact non-disordered DOS [13] along with the recursion method result. The non-disordered DOS of the unbiased bilayer (dashed line) falls linearly when $|E| \rightarrow 0$, being finite at zero energy [11, 13]. When the layers are made inequivalent by the bias a gap opens and 1D-like divergences associated with the “Mexican hat” like dispersion region show up [14]. The recursion method reproduces this behavior fairly well, in spite of a somewhat underestimated gap (dotted vertical lines signal the exact the gap limits). In Fig. 2 (b) we show the DOS for several disorder values. The disorder parameter W equals the relevant energy scales of the problem: bias, V ; inter-plane hopping, t_{\perp} ; and in-plane hopping t . It is readily seen that the disordered DOS starts to depart from the non-disordered one only for $W \sim t$. Figure 2 (c) is our main result of this section, and shows the disordered DOS in the gap region. Diagonal disorder closes the gap when its width is of the order of the largest energy scale in the system, $W \sim t$.

IV. MAGNETIC FIELD EFFECTS

We have computed the cyclotron effective mass $m_c^*(n)$, whose semi-classical expression is given by $m_c^*(n) = (\hbar^2/2\pi)\partial A(E)/\partial E|_{E=E_F(n)}$, where $A(E)$ is the k -space area enclosed by the orbit of energy E and n is the carrier density at the Fermi energy E_F . Its dependence on the carrier density n may be found through measurements of Shubnikov de Haas oscillations. Here we consider only the experimentally relevant case $V \ll t_{\perp} \ll t$, and we further assume that the inequality $E_F \ll t$ holds. In that case the Dirac linear dispersion can be used for $\epsilon_{\mathbf{k}}$ in Eq. (3), and analytical expressions for the cyclotron effective mass may be derived. When E_F is varied we have to distinguish three different cases (see Fig. 2): for $|E_F|$ in the “Mexican hat” region, $|E_F| < V/2$, there are two types of quasi-particles with Fermi wave vectors q_F^+ and q_F^- (relatively to Dirac points) and opposite cyclotron effective masses; when $|E_F|$ is between the top of the “Mexican hat” and the bottom of the high energy band, $V/2 < E_F < (t_{\perp}^2 + V^2/4)^{1/2}$, only q_F^+ quasi-particles exist; q_F^- quasi-particles show up again for $E_F > (t_{\perp}^2 + V^2/4)^{1/2}$ with positive cyclotron effective mass. The Fermi wave vectors are functions of the Fermi energy, $taq_F^{\pm} = (2/\sqrt{3})\{E_F^2 + V^2/4 \pm [E_F^2(V^2 + t_{\perp}^2) - t_{\perp}^2 V^2/4]^{1/2}\}^{1/2}$, and the respective cyclotron effective masses are given by,

$$m_c^{\pm} = \frac{\hbar^2}{a^2 t^2} \frac{2}{3} \left[2E_F \pm \frac{E_F(V^2 + t_{\perp}^2)}{\sqrt{E_F^2(V^2 + t_{\perp}^2) - t_{\perp}^2 V^2/4}} \right], \quad (5)$$

where the Fermi energy depends on the density as,

$$E_F = \begin{cases} \sqrt{\frac{(\frac{3\pi}{8}\tilde{n})^2 + \frac{t_{\perp}^2 V^2}{4}}{V^2 + t_{\perp}^2}} & \tilde{n} < \frac{4}{3\pi} V^2 \\ \sqrt{\frac{3\pi}{4}\tilde{n} + \frac{t_{\perp}^2}{2} + \frac{V^2}{4}} - \sqrt{\frac{t_{\perp}^4}{4} + (t_{\perp}^2 + V^2)\frac{3\pi}{4}\tilde{n}} & \frac{4}{3\pi} V^2 < \tilde{n} < \frac{4}{3\pi}(2t_{\perp}^2 + V^2) \\ \sqrt{\frac{3\pi}{8}\tilde{n} - \frac{V^2}{4}} & \tilde{n} > \frac{4}{3\pi}(2t_{\perp}^2 + V^2) \end{cases}, \quad (6)$$

with $\tilde{n} = a^2 t^2 n$. Figure 3 shows the result for m_c^+ [Eq. (5)] as a function of the carrier density; $n < 0$ for holes and $n > 0$ for electrons. As can be seen for $V/t = 0.01 \approx 27$ (meV) – full line – there is a $1/n$ behavior for small densities, which is associated with the presence of the “Mexican hat” dispersion [13], and for higher densities the cyclotron mass increases as the

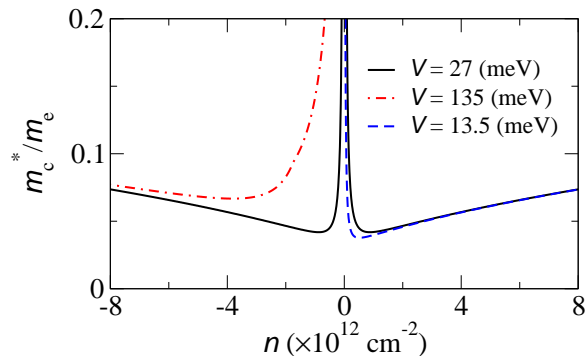


FIG. 3: (Color online) Cyclotron effective mass m_c^+ [given in Eq. (5)] in units of the bare electron mass, m_e , as a function of the carrier density for three different bias values. We set $t_\perp/t = 0.1$

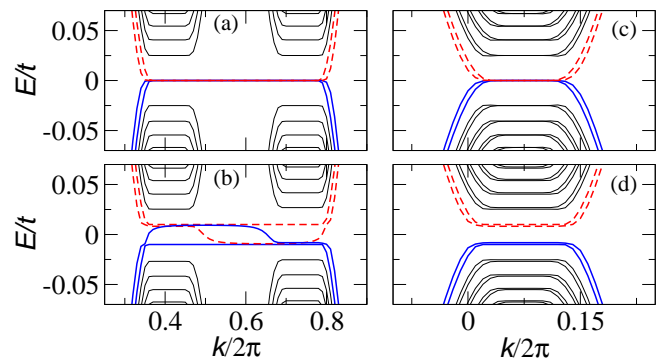


FIG. 4: (Color online) Energy spectrum for a ribbon of bilayer graphene with zigzag (a-b) and armchair (c-d) edges and width $N = 400$ unit cells: (a-c) – $V = 0$; (b-d) – $V = t_\perp/10$. We set $B = 30$ T and $t_\perp/t = 0.2$.

carrier density increases. It is worth mentioning that a more realistic calculation would account for the variations of the bias with the density, $V(n)$, as varying one implies the variation of the other. We postpone to future work the problem of the determination of $V(n)$ [13]. Also, the bias may not be the same for equal concentration of holes and electrons [7, 8]. In that case the cyclotron effective mass is asymmetric with respect to doping with holes or electrons. This is clearly seen in Fig. 3, where we show m_c^+ for $V/t = 0.05 \approx 135$ (meV) – holes – and $V/t = 0.005 \approx 13.5$ (meV) – electrons.

Landau level formation in bilayer graphene was already studied in the continuum limit in Ref. [6]. Here we study the problem of a bilayer subjected to a perpendicular magnetic field using the tight-binding Hamiltonian given by Eq. (1), both at zero and finite bias. Again we assume that inequalities $V \ll t_\perp \ll t$ hold. Bilayer nano-ribbons with zigzag and armchair edges were diagonalized, the obtained spectrum is shown in Fig. 4. For each k , the momentum parallel to the edge, there are $4N$ bands. In Fig. 4, however, we focus on the low energy behavior near the Dirac points. Panels (a) and (c) show the result for the unbiased bilayer with zigzag and armchair edges, respectively. Fourfold degenerate zero energy Landau levels are clearly seen, along with twofold degenerate non-zero Landau levels, in agreement with the continuum result [6]. The major difference between zigzag and armchair is that the former have zero energy surface states along with zero energy bulk Landau levels [13]. The result for the biased bilayer, $V = t_\perp/10 = 0.02$, is shown in panels (b) and (d) for zigzag and armchair edges, respectively. The fourfold degeneracy of zero energy Landau levels is lifted. A gap V opens and twofold degenerate Landau levels at $V/2$ and $-V/2$ show up. In fact it can be shown that their wave functions are either localized in layer 1 or 2. For zigzag edges it becomes clear that surface states and bulk Landau levels of the same band live in different layers [13]. As a consequence, dispersive surface states appear inside the gap, as shown in Fig. 4 (d).

V. CONCLUSIONS

Using a tight-binding approximation we have studied the electronic behavior of a graphene bilayer with layers at different electrostatic potential – *biased bilayer*. The applied bias opens a gap in the spectrum which is completely controlled by the applied voltage. We have shown that diagonal disorder reduces the size of the gap, which finally closes when the width of the disorder distribution equals the larger energy scale in the system: the in-plane hopping t . We have also studied the biased bilayer in the presence of a perpendicular magnetic field. We have calculated the semi-classical cyclotron effective mass as a function of the carrier density and bias, which is valid for low magnetic fields. When the field is sufficiently high Landau level formation in zigzag and armchair nano-ribbons is perfectly seen, where a gap between the lowest electron-like and the highest hole-like bulk Landau levels opens in the presence of a finite bias.

We thank A. H. Castro Neto and F. Guinea for many illuminating discussions. E.V.C. acknowledges the financial support of Fundação para a Ciência e a Tecnologia through Grant No. SFRH/BD/13182/2003. J.M.B.L.S. and E.V.C. were additionally financed by FCT and EU through POCTI (QCAIII). N.M.R.P. is thankful to the ESF Science Programme

No. INSTANS 2005-2010 and FCT and EU under the Grant No. POCTI/FIS/58133/2004.

- [1] K. S. Novoselov, A. K. Geim, S. V. Morozov, D. Jiang, Y. Zhang, S. V. Dubonos, I. V. Grigorieva, and A. A. Firsov, *Science* **306**, 666 (2004).
- [2] K. S. Novoselov, A. K. Geim, S. V. Morozov, D. Jiang, M. I. Katsnelson, I. V. Grigorieva, S. V. Dubonos, and A. A. Firsov, *Nature* **438**, 197 (2005).
- [3] Y. Zhang, Y.-W. Tan, H. L. Stormer, and P. Kim, *Nature* **438**, 201 (2005).
- [4] N. M. R. Peres, F. Guinea, and A. H. Castro Neto, *Phys. Rev. B* **73**, 125411 (2006).
- [5] K. S. Novoselov, E. McCann, S. V. Morozov, V. I. Fal'ko, M. I. Katsnelson, U. Zeitler, D. Jiang, F. Schedin, and A. K. Geim, *Nature Physics* **2**, 177 (2006).
- [6] E. McCann and V. I. Fal'ko, *Phys. Rev. Lett.* **96**, 086805 (2006).
- [7] A. K. Geim, private communication.
- [8] T. Ohta, A. Bostwick, T. Seyller, K. Horn, and E. Rotenberg, *Science* **313**, 951 (2006).
- [9] J. Nilsson, A. H. Castro Neto, F. Guinea, and N. M. R. Peres, cond-mat/0607343.
- [10] R. Peierls, *Z. Phys.* **80**, 763 (1933).
- [11] J. Nilsson, A. H. Castro Neto, F. Guinea, and N. M. R. Peres, cond-mat/0604106.
- [12] R. Haydock, in: *Solid State Physics*, edited by H. Ehrenreich, F. Seitz, and D. Turnbull, Vol. 35, (Academic Press, New York, 1980), p. 215.
- [13] E. V. Castro *et al.*, in preparation.
- [14] F. Guinea, A. H. Castro Neto, and N. M. R. Peres, *Phys. Rev. B* **73**, 245426 (2006).